Original Article

Impact of deep learning-based image reconstruction on image quality and lesion visibility in renal computed tomography at different doses

Yifan Bie^, Shuo Yang, Xingchao Li, Kun Zhao, Changlei Zhang, Hai Zhong^

Department of Radiology, the Second Hospital, Shandong University, Jinan, China

Contributions: (I) Conception and design: Y Bie, H Zhong; (II) Administrative support: H Zhong; (III) Provision of study materials or patients: X Li, K Zhao, C Zhang; (IV) Collection and assembly of data: Y Bie, S Yang; (V) Data analysis and interpretation: Y Bie, S Yang, H Zhong; (VI) Manuscript writing: All authors; (VII) Final approval of manuscript: All authors.

Correspondence to: Hai Zhong. Department of Radiology, the Second Hospital, Shandong University, 247# Beiyuan Road, Jinan 250033, China. Email: 18753107255@163.com.

Background: Numerous computed tomography (CT) image reconstruction algorithms have been developed to improve image quality, and high-quality renal CT images are crucial to clinical diagnosis. This study evaluated the image quality and lesion visibility of deep learning-based image reconstruction (DLIR) compared with adaptive statistical iterative reconstruction-Veo (ASiR-V) in contrast-enhanced renal CT at different reconstruction strengths and doses.

Methods: From January 2020 to May 2021, we prospectively included 101 patients who underwent renal contrast-enhanced CT scanning (69 at 120 kV; 32 at 80 kV). All image data were reconstructed with ASiR-V (30% and 70%) and DLIR at low, medium, and high reconstruction strengths (DLIR-L, DLIR-M, and DLIR-H, respectively). The CT number, noise, noise reduction rate (NRR), signal-to-noise ratio (SNR), contrast-to-noise ratio (CNR), overall image quality, and the proportion of acceptable images were compared. Lesions of DLIR groups were evaluated, and the conspicuity-to-noise ratio (C/N) was calculated.

Results: Quantitative values (noise, SNR, CNR, and NRR) significantly differed between all reconstructions at 120 and 80 kV (P<0.001) and between each reconstruction, except ASiR-V 70% *vs.* DLIR-M. At 120 kV, the overall image quality and the proportion of acceptable images significantly differed between all reconstructions (P<0.001) and between each reconstruction, except ASiR-V 30% *vs.* DLIR-L and ASiR-V 70% *vs.* DLIR-M. At 80 kV, the overall image quality significantly differed between all reconstructions (P<0.001) and between each reconstruction, except between ASiR-V 30%, ASiR-V 70%, and DLIR-L. Quantitative and qualitative values were highest in DLIR-H, while the values were close in DLIR-H (80 kV) *vs.* ASiR-V 70% (120 kV) and DLIR-M (80 kV) *vs.* ASiR-V 30% (120 kV). The lesion conspicuity and noise significantly differed in DLIR at 120 kV and 80 kV (P<0.001). C/N significantly differed in DLIR at 120 kV (P<0.001) but not at 80 kV. DLIR-L and DLIR-M exhibited much-improved lesion display (C/N >1), and DLIR-H exhibited much-improved noise (C/N <1) at 120 kV.

Conclusions: DLIR significantly improved the image quality and lesion visibility of renal CT compared with ASiR-V, even at a low dose.

Keywords: Deep learning image reconstruction; adaptive statistical iterative reconstruction-Veo (ASiR-V); image quality; tomography; kidney

^ ORCID: Yifan Bie, 0000-0001-9169-4287; Hai Zhong, 0000-0001-7530-6862.

Submitted Aug 13, 2022. Accepted for publication Jan 20, 2023. Published online Feb 15, 2023.
doi: 10.21037/qims-22-852
View this article at: https://dx.doi.org/10.21037/qims-22-852

Introduction

As a first-line imaging technology for detecting renal lesions, computed tomography (CT) involves a short examination time and is low cost (1). However, artifacts that might be generated during CT imaging affect the diagnosis of kidney diseases (2). Given the diverse manifestations of renal lesions and the relatively complex multiphase scanning scheme, high-quality renal CT images are necessary for accurate diagnosis. Adaptive statistical iterative reconstruction-Veo (ASiR-V) was developed based on a physical model of an iterative reconstruction process, resulting in improved image quality and noise reduction (3). However, some studies revealed that ASiR-V images might be limited by a waxy, plastic, and unnatural appearance (4,5). Artificial intelligence in medical imaging can distinguish noise from anatomical structures and remove that noise from the raw image to achieve better image quality and decrease the radiation dose (4,6). By improving the ability to identify anatomical structures, deep learning-based image reconstruction (DLIR; TrueFidelity, GE Healthcare) can significantly improve image quality compared with traditional model-based iterative reconstruction methods (5,7,8). DLIR has been applied to some phantom and clinical studies, providing satisfactory noise reduction and better image quality than those of ASiR-V (9-11). This study evaluated the impact of DLIR algorithms on renal CT image quality and lesions at a routine dose (120 kV) and a low dose (80 kV).

Methods

Patients

From January 2020 to May 2021, 101 patients with enhanced renal CT scanning images were included in this prospective study. As the radiation dose received by patients can vary, scans of different doses were performed (69 cases in the routine-dose group at 120 kV; 32 cases in the low-dose group at 80 kV). Patients were included if they planned to undergo an enhanced renal CT examination and had a normal weight, with a body mass index (BMI) of 18.5–23.9 kg/m^2 as recommended for Chinese adults (12). Patients were excluded if they had a severe allergy to iodized contrast media, had cardiac insufficiency, were pregnant, or had impaired renal function (glomerular filtration rate <60 mL/min/1.73 m^2). The study was conducted in accordance with the Declaration of Helsinki (as revised in 2013). The study was approved by Shandong University, and informed consent was obtained from all the patients.

CT data acquisition and image reconstruction

A 256-row CT scanner (Revolution CT; GE Healthcare, Chicago, IL, USA) was used for scanning. The main scanning parameters were the following: scanning mode, spiral; pitch, 0.992:1; noise index, 8.0; collimation, 1.25 mm; tube rotation time, 0.5 s; routine-dose group, 120 kV/SmartmA (100–500 mA); and low-dose group, 80 kV/SmartmA (100–600 mA). After the precontrast phase, the abdominal aorta at the level of the porta hepatis was monitored for threshold trigger scanning. The trigger threshold was 120 HU. The corticomedullary, nephrographic, and excretory phases were initiated with delays of 30 s, 70 s, and 3 min, respectively, according to a bolus-tracking program (SmartPrep; GE Healthcare). The amount of nonionic contrast agent containing 300 mg iodine/mL was 1.5 mL/kg for patients' body weight (450 mg iodine/kg) and was injected at a rate of 3.0 mL/s. The renal nephrographic phase images were reconstructed at 120 and 80 kV using ASiR-V (30% and 70%) and DLIR at low, medium, and high reconstruction strengths (DLIR-L, DLIR-M, and DLIR-H, respectively). The reconstruction thickness and interval were 1.25 mm.

Radiation dose

The volume CT dose index (CTDIvol; mGy) and the scanning dose-length product (DLP; mGy·cm) in the nephrographic phase of the dose report were recorded, and the effective dose (ED) was calculated with k=0.015 mSv/(mGy·cm) (13).

Quantitative image analysis

Image analysis was performed on Advantage Workstation 4.6 (GE Healthcare). All patient information and scanning

Table 1 Grading scores of qualitative image assessments

Grading score	Differentiation of renal boundary	Conspicuity of renal hilum	Sharpness	Artifacts	Subjective noise	Lesion conspicuity	Overall image quality
1	Non-diagnostic	Non-diagnostic	Blurry	Marked	Marked	Non-diagnostic	5 (worst)
2	Poor	Poor	Slight	Major	Major	Poor	≥12 (acceptable)
3	Moderate	Moderate	Strong	Minor	Minor	Moderate	20 (best)
4	Excellent	Excellent	Distinct	Absent	Absent	Excellent	

parameters were hidden. The reconstructed images were linked to enable the simultaneous review of identical anatomic levels. The region of interest (ROI) used had a diameter of 3 to 5 mm, bilateral measurements were repeated twice, and the average values were recorded. A radiologist with more than 3 years of working experience drew the ROIs on the subcutaneous fat of the abdominal wall, bilateral renal parenchyma, and proximal renal vein at the level of the renal hilum. Measurements avoided calcification, thrombosis, local lesions, and artifacts. The CT number and noise of each measurement were recorded. The noise of subcutaneous fat was included as the background noise.

The signal-to-noise ratio (SNR) was calculated as follows:

$$SNR=HU_{target}/Noise_{target} \quad [1]$$

The contrast-to-noise ratio (CNR) relative to fat was calculated as follows (14):

$$CNR=\left(\text{mean } HU_{target}-\text{mean } HU_{fat}/Noise_{fat}\right) \quad [2]$$

The noise reduction rate (NRR) relative to ASiR-V 30% was calculated as follows:

$$NRR=\left(Noise_{ASiR\text{-}V\ 30\%}-Noise_{target}\right)/Noise_{ASiR\text{-}V\ 30\%}\times 100\% \quad [3]$$

Qualitative image analysis

Two radiologists with 5 years of experience performed blind evaluations, 1 of whom repeated the evaluation after 2 weeks. In cases of discordance between the two radiologists, a final consensus was achieved. The 4-point subjective scale (1 to 4 points) was used (*Table 1*) to grade the differentiation of the renal boundary, the conspicuity of the renal hilum, sharpness, artifacts, and subjective noise. The overall image quality based on the above 5 aspects was calculated, with the total score ranging from 5 (worst) to 20 (best). When the overall image quality score was ≥12, which was more than 60% of the maximum of the overall image quality score, the images were considered to be of acceptable diagnostic quality (15). Correspondingly, the proportion of acceptable images was calculated.

DLIR lesion evaluation

Cases with renal lesions of DLIR at 120 and 80 kV groups were evaluated. The lesions included suspected primary tumors, metastases, and other cystic or solid lesions. The lesion conspicuity and noise were graded (*Table 1*), and the conspicuity-to-noise ratio (C/N) at every reconstruction strength was calculated as follows:

$$C/N=score_{conspicuity}/score_{noise} \quad [4]$$

C/N was used to evaluate the varying degrees of improvement in lesion conspicuity and noise reduction at different reconstruction strengths. When the images showed much-improved details of lesion visibility, C/N >1. When the images showed much-improved decreasing noise, C/N <1.

Statistical analysis

SPSS 19.0 (IBM Corp., Armonk, NY, USA) was used for statistical analysis. The data are expressed as the mean ± standard deviation. After using the Kolmogorov-Smirnov test to determine if the data followed a normal distribution, analysis of variance (ANOVA) was used to compare differences. For the evaluation between lesions and the reconstruction strength, a linear trend was tested with the Cochran-Armitage trend test. The Kruskal-Wallis test was used for data that did not conform to a normal distribution. Intraclass correlation (ICC) analysis was used to evaluate the consistency between and within observers. ICC <0.4, 0.4–0.8, and >0.8 indicated weak, moderate, and strong agreement, respectively. A 2-tailed P value <0.05 was considered statistically significant.

Table 2 Radiation doses and characteristics of participants

Voltage	CTDIvol (mGy)	DLP (mGy·cm)	ED (mSv)	Age (years)	Sex	BMI (kg/m^2)
120 kV	11.89±4.96	363.96±190.24	5.50±2.85	59.38±0.95	45 M, 24 F	23.45±2.09
80 kV	2.53±0.82	77.02±28.22	1.15±0.42	61.02±1.09	20 M, 12 F	19.84±2.41
P value	<0.001	<0.001	<0.001	0.198	0.791	0.196

Data are given as mean ± standard deviation. CTDIvol, volume CT dose index; DLP, dose length product; ED, effective dose; M, male; F, female; BMI, body mass index.

Results

Characteristics of participants and radiation dose

There were 101 cases evaluated in this study (59.93±1.26 years; 65 males; 36 females; BMI 22.24±2.78 kg/m^2). In the 120 kV group (69 cases), the DLP was 363.96±190.24 mGy·cm, the CTDIvol was 11.89±4.96 mGy, and the ED was 5.50±2.85 mSv. In the 80 kV group (32 cases), the DLP was 77.02±28.22 mGy·cm, the CTDIvol was 2.53±0.82 mGy, and the ED was 1.15±0.42 mSv. There were no significant differences in age, sex, or BMI between the 120 and 80 kV groups (P>0.05), while the difference in radiation doses was statistically significant (P<0.001) (*Table 2*). The radiation dose in the 80 kV group was 79% lower than that in the 120 kV group (P<0.001).

Quantitative image analysis

Noise, SNR, CNR, and NRR were significantly different between the 5 reconstructions at both 120 and 80 kV (P<0.001) and between each reconstruction, except for ASiR-V 70% *vs.* DLIR-M. Furthermore, DLIR-H exhibited the lowest noise and the highest SNR, CNR, and NRR at both 120 and 80 kV (*Table 3*; *Figure 1*).

Qualitative image analysis

The inter- and intraobserver correlation coefficients were 0.874 (95% confidence interval: 0.840–0.902; P<0.001) and 0.924 (95% confidence interval: 0.797–0.972; P<0.001), respectively (*Table 4*).

Overall image quality at 120 kV

The overall image quality and the proportion of acceptable images were significantly different between the 5 reconstructions (P<0.001) and between each reconstruction, except for ASiR-V 30% *vs.* DLIR-L and ASiR-V 70% *vs.* DLIR-M. The overall image quality and the proportion of acceptable images were as follows (from the highest to the lowest): DLIR-H, DLIR-M, ASiR-V 70%, DLIR-L, and ASiR-V 30% (*Table 5*; *Figure 2*).

Overall image quality at 80 kV

The overall image quality was significantly different between 5 reconstructions (P<0.001) and between each reconstruction, except among ASiR-V 30%, ASiR-V 70%, and DLIR-L. Differences in the proportion of acceptable images were statistically significant between the 5 reconstructions (P<0.05) and between each reconstruction. The overall image quality and the proportion of acceptable images were as follows (from the highest to the lowest): DLIR-H, DLIR-M, DLIR-L, ASiR-V 70%, and ASiR-V 30% (*Table 5*; *Figure 2*).

Comparisons between the DLIR groups at 80 kV and the ASiR-V groups at 120 kV

Significant differences were identified in noise, SNR, CNR, overall image quality, and the proportion of acceptable images between the DLIR groups at 80 kV and ASiR-V at 120 kV (P<0.001). However, there were no significant differences between DLIR-H at 80 kV and ASiR-V 70% at 120 kV or between DLIR-M at 80 kV and ASiR-V 30% at 120 kV (*Tables 3*,*5*; *Figures 1*,*2*).

Evaluation of lesions of DLIR

A total of 45 cases with renal lesions (30 and 15 cases in the 120 and 80 kV DLIR groups, respectively) and 103 lesions were evaluated (83 and 30 lesions in the 120 and 80 kV DLIR groups, respectively).

The lesion conspicuity, noise, and C/N significantly differed between DLIR reconstruction strengths at 120 kV (P=0.01; P<0.001; P<0.001). For the lesion conspicuity, noise, and C/N at 120 kV, significant linear trends dependent on DLIR reconstruction strengths were confirmed (P_{trend} =0.005; P_{trend} <0.001; P_{trend} <0.001). The C/N for DLIR-L, DLIR-M, and DLIR-H was 1.37, 1.06,

Table 3 Quantitative image analysis using ASiR-V and DLIR

Groups	CT number (HU)			$Noise_{fat}$	NRR (%)	SNR		CNR	
	Renal parenchyma	Renal vein	Fat			Renal parenchyma	Renal vein	Renal parenchyma	Renal vein
120 kV									
ASiR-V 30%	141.04±20.09	103.04±17.57	−102.61±5.91	13.11±3.16$^{++,*,**,***}$	–	6.72±1.57$^{++,*,**,***}$	4.88±1.47$^{++,*,**,***}$	19.63±4.01$^{++,*,**,***}$	16.26±3.67$^{++,*,**,***}$
ASiR-V 70%	140.95±19.93	102.25±16.47	−99.30±8.54	7.68±2.25$^{+,*,***}$	43.53*,***	11.65±3.29$^{+,*,***}$	8.37±1.53$^{+,*,***}$	34.48±9.79$^{+,*,***}$	28.82±8.20$^{+,*,***}$
DLIR-L	141.94±18.90	104.42±17.11	−99.39±11.28	9.39±2.02$^{+,++,**,***}$	25.63$^{++,**,***}$	8.87±2.02$^{+,++,**,***}$	6.08±1.21$^{+,++,**,***}$	27.63±6.38$^{+,++,**,***}$	22.76±5.36$^{+,++,**,***}$
DLIR-M	143.04±21.17	104.48±17.04	−98.00±12.06	7.41±1.55$^{+,*,***}$	44.71*,***	10.92±2.53$^{+,*,***}$	7.46±1.98$^{+,*,***}$	34.20±8.12$^{+,*,***}$	28.83±6.65$^{+,*,***}$
DLIR-H	143.22±21.37	105.36±16.68	−99.97±9.47	5.47±1.45$^{+,++,*,***}$	59.94$^{++,*,**}$	14.58±3.37$^{+,++,*,**}$	10.95±2.66$^{+,++,*,**}$	46.79±12.09$^{+,++,*,**}$	39.13±9.35$^{+,++,*,**}$
P value	0.981	0.942	0.509	<0.001	<0.001	<0.001	<0.001	<0.001	<0.001
80 kV									
ASiR-V 30%	151.13±17.29	97.29±15.45	−97.26±13.29	25.05±4.92$^{++,*,**,***}$	–	4.66±0.83$^{++,*,**,***}$	3.16±0.76$^{++,*,**,***}$	10.25±2.17$^{++,*,**,***}$	7.99±1.75$^{++,*,**,***}$
ASiR-V 70%	149.69±19.35	96.33±14.85	−100.28±10.07	13.89±2.62$^{+,*,***}$	44.68*,***	7.75±2.52$^{+,*,***}$	5.48±1.43$^{+,*,***}$	19.51±4.01$^{+,*,***}$	15.13±3.14$^{+,*,***}$
DLIR-L	151.48±20.49	99.04±15.91	−102.39±5.03	18.98±3.75$^{+,++,**,***}$	24.63$^{++,*,***}$	5.73±1.15$^{+,++,**,***}$	3.92±0.75$^{+,++,**,***}$	14.23±2.92$^{+,++,**,***}$	11.26±2.26$^{+,++,**,***}$
DLIR-M	151.24±20.82	98.64±15.92	−100.04±8.67	13.94±2.73$^{+,*,***}$	43.67*,***	7.30±1.48$^{+,*,***}$	5.06±0.92$^{+,*,***}$	19.12±4.28$^{+,*,***}$	15.23±3.38$^{+,*,***}$
DLIR-H	151.26±20.37	98.84±15.71	−102.34±4.59	8.77±1.91$^{+,++,*,***}$	65.76$^{++,*,**}$	10.42±2.17$^{+,++,*,**}$	7.49±1.50$^{+,++,*,**}$	32.14±6.35$^{+,++,*,**}$	25.24±4.85$^{+,++,*,**}$
P value	0.995	0.928	0.225	<0.001	<0.001	<0.001	<0.001	<0.001	<0.001

The data are shown as the mean ± standard deviation. Significant differences (P<0.05) *vs.* ASiR-V 30% (+), *vs.* ASiR-V 70% (++), *vs.* DLIR-L (*), *vs.* DLIR-M (**), and *vs.* DLIR-H (***) are shown. ASiR-V 30%/70%, adaptive statistical iterative reconstruction-Veo 30%/70%; DLIR-L, deep learning-based image reconstruction at low reconstruction strength; DLIR-M, deep learning-based image reconstruction at medium reconstruction strength; DLIR-H, deep learning-based image reconstruction at high reconstruction strength; NRR, noise reduction rate relative to ASiR-V 30%; SNR, signal-to-noise ratio; CNR, contrast-to-noise ratio.

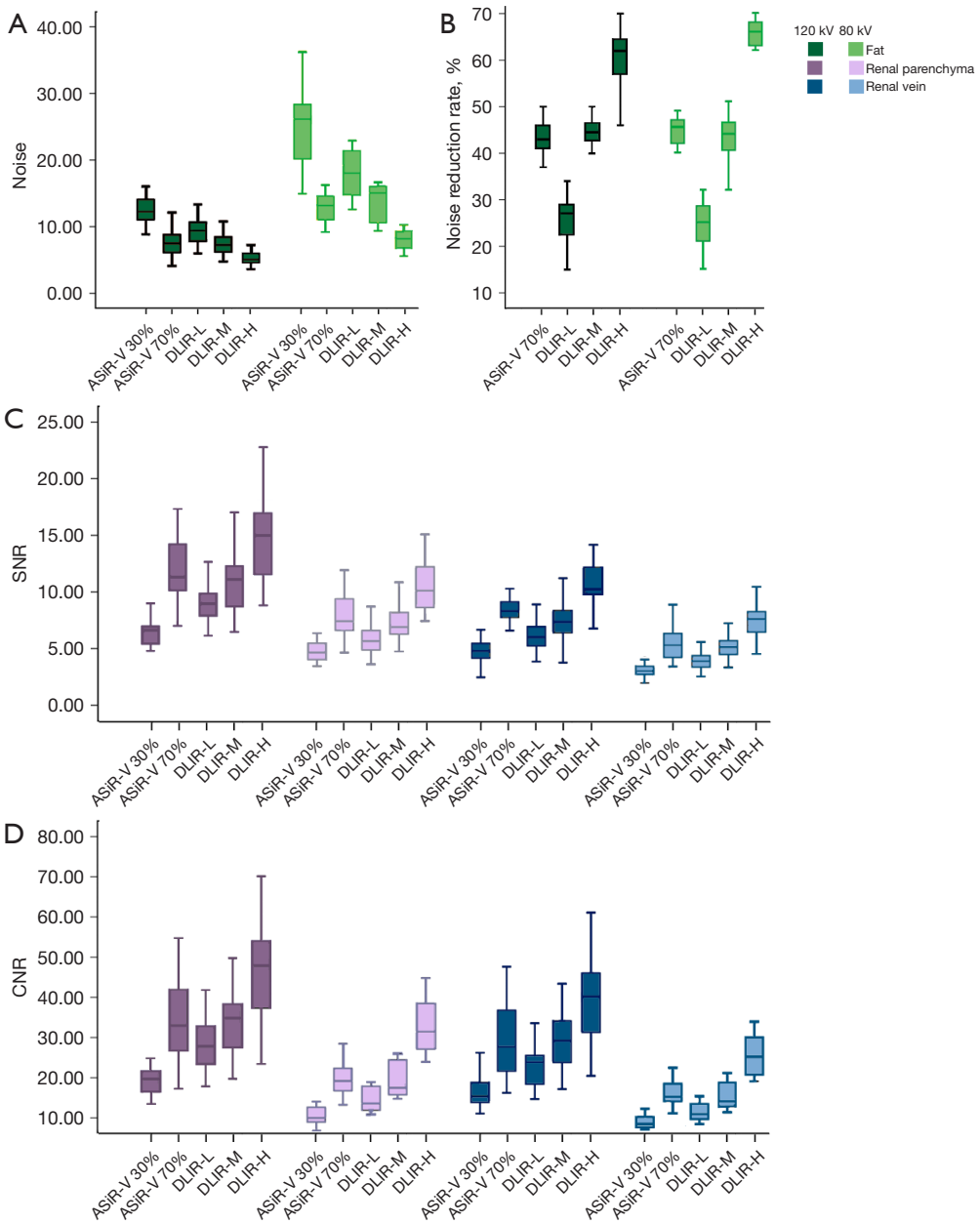

Figure 1 Quantitative image analysis of ASiR-V and DLIR. At 120 and 80 kV, noise, SNR, and CNR were significantly different between all reconstructions (P<0.001) and were also statistically significant between each reconstruction, except ASiR-V 70% *vs*. DLIR-M. ASiR-V 30%/70%, adaptive statistical iterative reconstruction-Veo 30%/70%; DLIR-L, deep learning-based image reconstruction at low reconstruction strength; DLIR-M, deep learning-based image reconstruction at medium reconstruction strength; DLIR-H, deep learning-based image reconstruction at high reconstruction strength; SNR, signal-to-noise ratio; CNR, contrast-to-noise ratio.

and 0.87, respectively.

The conspicuity of lesions and noise were significantly different between the DLIR reconstruction strengths at 80 kV (P<0.001; P<0.001), but C/N was not significantly different (P=0.941). For the lesion conspicuity and noise at 80 kV, significant linear trends dependent on DLIR reconstruction strengths were confirmed (P<0.001; P<0.001), but not for C/N (P_{trend}=0.758; *Table 6*; *Figure 2*).

Table 4 Qualitative image analysis using ASiR-V and DLIR

Groups	Differentiation of renal boundary		Conspicuity of renal hilum		Sharpness		Artifacts		Subjective noise	
	Rater 1	Rater 2	Rater 1	Rater 2	Rater 1	Rater 2	Rater 1	Rater 2	Rater 1	Rater 2
120 kV										
ASiR-V 30%	3.81±0.40	3.24±0.54	3.44±0.62	2.92±0.45	3.53±0.51	3.85±0.36	2.97±0.65	2.50±0.58	2.84±0.37	2.77±0.42
ASiR-V 70%	3.84±0.37	3.69±0.47	3.81±0.40	3.71±0.51	2.66±0.48	2.56±0.54	3.47±0.62	2.94±0.60	3.53±0.57	3.15±0.58
DLIR-L	3.88±0.34	3.39±0.49	3.63±0.55	2.89±0.31	3.72±0.46	3.54±0.62	3.22±0.61	2.55±0.51	3.09±0.39	2.77±0.67
DLIR-M	3.90±0.30	3.63±0.53	3.84±0.37	3.71±0.54	3.88±0.42	2.78±0.47	3.75±0.51	3.23±0.69	3.59±0.50	3.31±0.47
DLIR-H	3.97±0.18	3.83±0.38	3.91±0.30	3.79±0.46	2.81±0.47	2.08±0.65	3.88±0.34	3.67±0.56	3.97±0.18	3.79±0.41
80 kV										
ASiR-V 30%	3.08±0.49	3.18±0.51	2.60±0.53	2.58±0.50	3.59±0.55	3.40±0.68	2.42±0.55	2.53±0.52	2.16±0.50	1.97±0.41
ASiR-V 70%	3.43±0.50	3.27±0.46	2.97±0.76	2.72±0.70	2.56±0.50	2.50±0.51	2.76±0.68	2.62±0.50	2.90±0.49	2.86±0.35
DLIR-L	3.29±0.57	3.37±0.56	2.76±0.79	2.54±0.64	3.47±0.65	3.43±0.63	2.63±0.54	2.68±0.55	2.39±0.64	2.32±0.55
DLIR-M	3.53±0.51	3.44±0.51	3.26±0.50	3.11±0.42	2.66±0.48	2.64±0.49	3.18±0.69	3.14±0.65	3.05±0.40	3.06±0.42
DLIR-H	3.61±0.50	3.73±0.45	3.45±0.50	3.21±0.57	2.63±0.49	2.57±0.50	3.42±0.60	3.39±0.57	3.66±0.48	3.71±0.46

The data are shown as the mean ± standard deviation. ASiR-V 30%/70%, adaptive statistical iterative reconstruction-Veo 30%/70%; DLIR-L, deep learning-based image reconstruction at low reconstruction strength; DLIR-M, deep learning-based image reconstruction at medium reconstruction strength; DLIR-H, deep learning-based image reconstruction at high reconstruction strength.

Table 5 Overall image quality using ASiR-V and DLIR

Groups	Overall image quality	Score ≥12 (%)
120 kV		
ASiR-V 30%	$13.48\pm1.54^{++,**,***}$	$60.42^{++,**,***}$
ASiR-V 70%	$16.06\pm1.80^{+,*,***}$	$89.58^{+,*,***}$
DLIR-L	$13.67\pm1.85^{++,**,***}$	$60.42^{++,**,***}$
DLIR-M	$16.40\pm1.65^{+,*,***}$	$93.75^{+,*,***}$
DLIR-H	$17.08\pm1.33^{+,++,*,**}$	$100^{+,++,*,**}$
P value	<0.001	<0.001
80 kV		
ASiR-V 30%	$12.84\pm1.4^{**,***}$	$32.00^{++,*,**,***}$
ASiR-V 70%	$12.86\pm1.83^{**,***}$	$40.91^{+,*,**,***}$
DLIR-L	$13.32\pm1.7^{**,***}$	$46.43^{+,++,**,***}$
DLIR-M	$14.36\pm1.66^{+,++,*,***}$	$60.71^{+,++,*,***}$
DLIR-H	$15.43\pm1.50^{+,++,*,**}$	$89.29^{+,++,*,**}$
P value	<0.001	0.012

The data are shown as the mean ± standard deviation. Significant differences (P<0.05) were *vs.* ASiR-V 30% (+), *vs.* ASiR-V 70% (++), *vs.* DLIR-L (*), *vs.* DLIR-M (**), and *vs.* DLIR-H (***) are shown. ASiR-V 30%/70%, adaptive statistical iterative reconstruction-Veo 30%/70%; DLIR-L, deep learning-based image reconstruction at low reconstruction strength; DLIR-M, deep learning-based image reconstruction at medium reconstruction strength; DLIR-H, deep learning-based image reconstruction at high reconstruction strength.

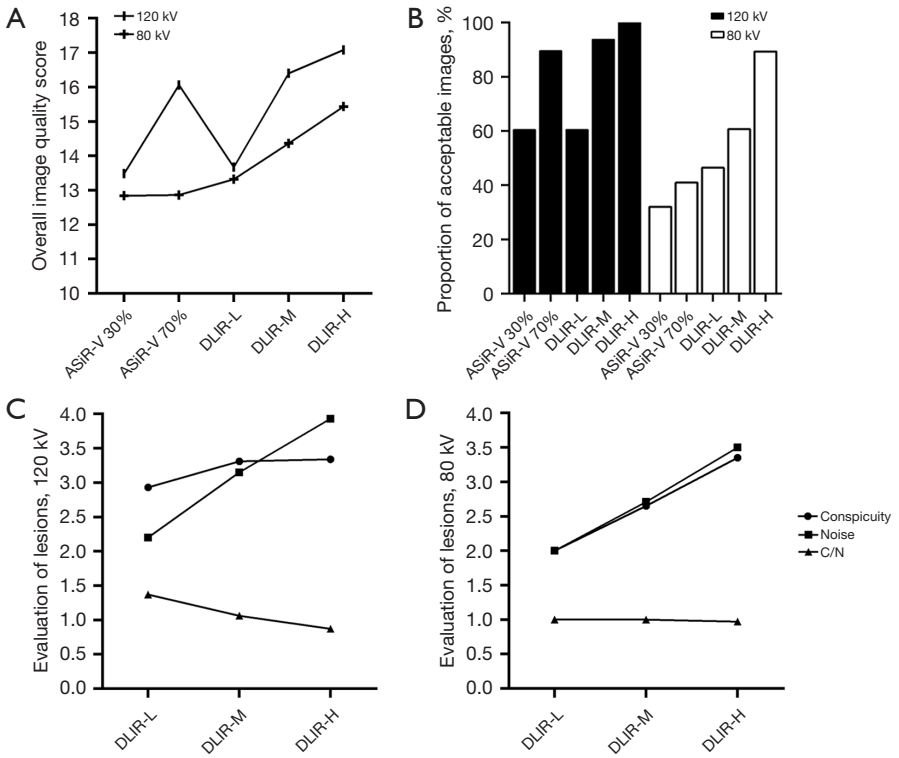

Figure 2 Overall image quality of ASiR-V and DLIR and the evaluation of lesions using DLIR. The overall image quality and the proportion of acceptable images were significantly different between each reconstruction at 120 kV, except ASiR-V 30% *vs*. DLIR-L and ASiR-V 70% *vs*. DLIR-M and significantly different between each reconstruction at 80 kV, except among ASiR-V 30%, ASiR-V 70%, and DLIR-L (A,B). The lesion conspicuity, noise, and C/N were significantly different between the DLIR groups at 120 kV (P<0.001) (C). The conspicuity of lesions and noise were significantly different between the DLIR groups at 80 kV (P<0.001), but C/N was not significantly different (D). ASiR-V 30%/70%, adaptive statistical iterative reconstruction-Veo 30%/70%; DLIR-L, deep learning-based image reconstruction at low reconstruction strength; DLIR-M, deep learning-based image reconstruction at medium reconstruction strength; DLIR-H, deep learning–based image reconstruction at high reconstruction strength; C/N, conspicuity-to-noise ratio.

Table 6 Evaluation of lesions in DLIR

Groups	Lesion conspicuity	Noise	C/N
120 kV			
DLIR-L	2.93±0.73**,***	2.20±0.50**,***	1.37±0.39**,***
DLIR-M	3.31±0.54*,***	3.15±0.36*,***	1.06±0.26*,***
DLIR-H	3.41±0.57*,**	3.93±0.26*,**	0.87±0.14*,**
P value	0.01	<0.001	<0.001
80 kV			
DLIR-L	2.00±0.89**,***	2.00±0.00**,***	1.00±0.45
DLIR-M	2.65±0.49*,***	2.71±0.47*,***	1.00±0.23
DLIR-H	3.35±0.49*,**	3.50±0.52*,**	0.97±0.85
P value	<0.001	<0.001	0.941

The data are shown as the mean ± standard deviation. Significant differences (P<0.05) *vs.* DLIR-L (*), *vs.* DLIR-M (**), and *vs.* DLIR-H (***) are shown. C/N, conspicuity-to-noise ratio; DLIR-L, deep learning-based image reconstruction at low reconstruction strength; DLIR-M, deep learning-based image reconstruction at medium reconstruction strength; DLIR-H, deep learning-based image reconstruction at high reconstruction strength.

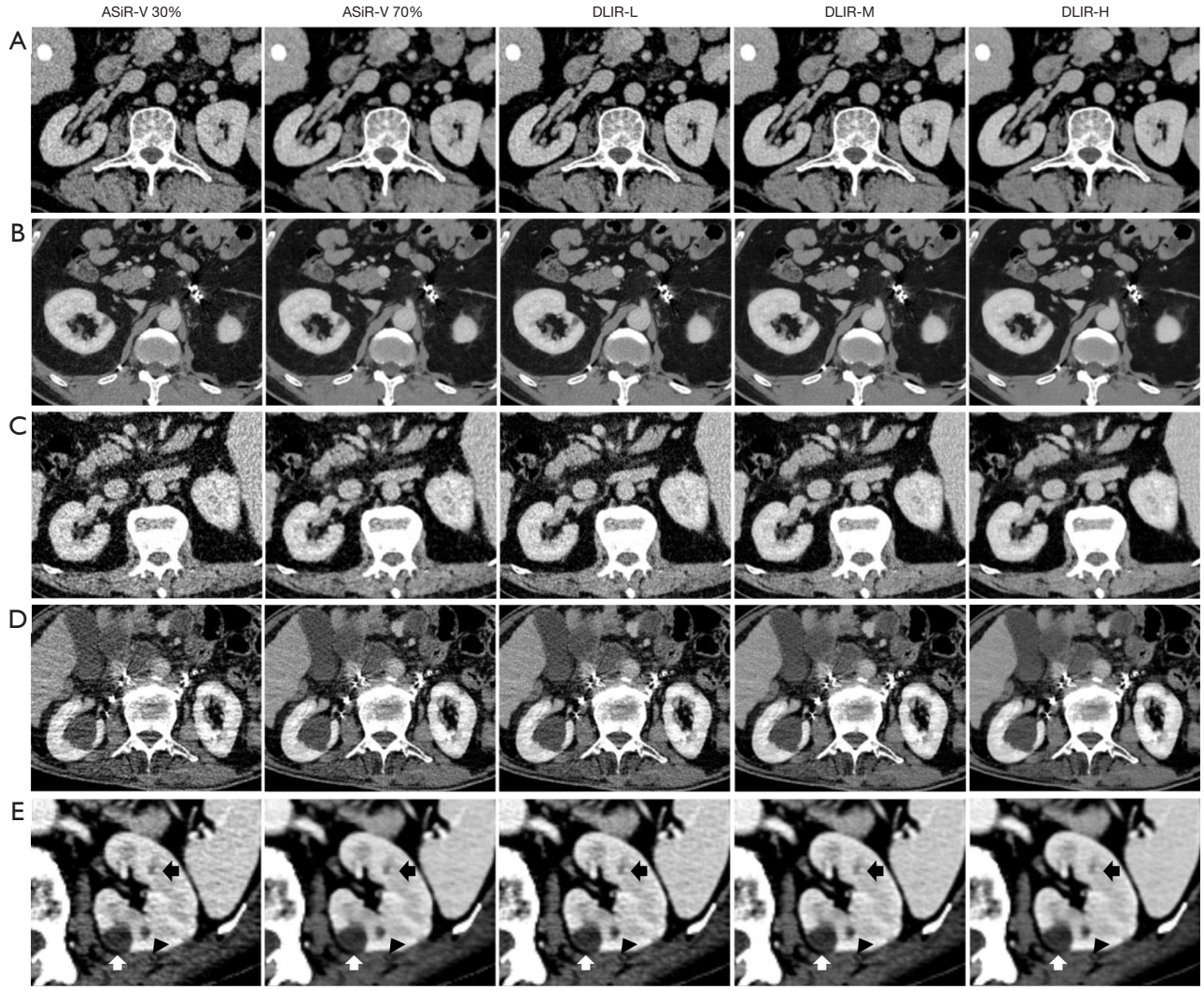

Figure 3 Image quality comparison of ASiR-V 30%, ASiR-V 70%, DLIR-L, DLIR-M, and DLIR-H. Images of DLIR and ASiR-V at 120 kV (A,B) and 80 kV (C,D). After intervention therapy in 2 patients, prominent radial and streak-like artifacts were apparent, and several ovoid hypoenhancing lesions were observed in the kidney (B,D). Three lesions of different sizes are marked with white arrows, black arrowheads, and black arrows. DLIR-H displayed slight blurring of lesions smaller than 5 mm (black arrow; E). ASiR-V 30%/70%, adaptive statistical iterative reconstruction-Veo 30%/70%; DLIR-L, deep learning-based image reconstruction at low reconstruction strength; DLIR-M, deep learning-based image reconstruction at medium reconstruction strength; DLIR-H, deep learning-based image reconstruction at high reconstruction strength.

Discussion

DLIR has the potential to reduce noise and improve image quality (3-6,14,15). Using DLIR could decrease the radiation dose and maintain diagnostic performance. In this study, compared with ASiR-V, DLIR not only improved the objective image quality (higher noise, NRR, SNR, and CNR) but also provided better subjective image quality (higher overall image quality score and a proportion of acceptable image). DLIR-H exhibited the best image quality, even at a low dose and with significant artifacts (*Figure 3*). The overall image quality and the proportion of acceptable image quality in DLIR-H and DLIR-M were higher than those of ASiR-V at both 120 and 80 kV. Moreover, DLIR-H had the highest level of noise reduction and subjective image quality. DLIR-H at 80 kV achieved an image quality close to that of ASiR-V 70% at 120 kV. These

results suggested that DLIR was better at identifying noise and optimizing images than was ASiR-V.

Based on prior studies, we evaluated the impact of DLIR on lesion visibility and noise (16,17). Trend tests are important for improving the performance of statistical and visual analysis (18,19). Accordingly, we tested and showed trends dependent on DLIR reconstruction strengths for lesion visibility and noise. We also introduced C/N to evaluate the differences in the improvement of lesion visibility and noise reduction. We found that the 2 were simultaneously improved but to varying degrees, as DLIR reconstruction strengths increased at 120 kV. At 120 kV, DLIR-L and DLIR-M (C/N >1) tended to optimize lesion conspicuity to a better degree than they reduced the noise. DLIR-H (C/N <1) tended to reduce the noise to a better degree than it optimized the lesion visibility. At 80 kV, the lesion display and noise reduction yielded increasing trends dependent on DLIR reconstruction strengths. However, it was hard to evaluate lesions based on relatively high-noise images, and the difference in improvement for both was not significant.

Previous studies reported that images using a high-strength denoising algorithm displayed a slight blurring, and the blurring of small lesions (<5 mm) at the highest reconstruction strength was revealed in DLIR (17,20,21) (*Figure 3E*). Our results showed that the improvement in noise reduction at DLIR-H might be better than the improvement in lesion display. This finding might explain the loss of details in DLIR-H images at the edges of small lesions. Therefore, DLIR-M might perform better than DLIR-H on small lesions with a 1.25-mm slice thickness. The strengths of DLIR in balancing the degree of lesions and denoising should be considered for clinical tasks (17).

This study had several limitations. First, the influence of DLIR on diagnostic accuracy and confidence under different pathological conditions still remains to be evaluated under specific diagnostic requirements. Second, the influences of applying DLIR to overall renal scanning remain to be explored in multiple phases. Third, only 1.25-mm images were evaluated in this study. Whether the blurring of small lesions could be improved at high reconstruction strength warrants studies with a thinner slice thickness. Fourth, C/N is a new concept, and its ability to improve to reveal the difference in improvement for lesion visibility and noise reduction at different DLIR reconstruction strengths needs to be confirmed in future studies. Fifth, although DLIR exhibited good image quality under low-dose renal CT scanning in a normal-weight population, its use in the overweight and obese population should be studied further. Finally, more raters are needed to conduct the subjective evaluations, and larger sample sizes are required to verify the conclusions of this study.

Conclusions

DLIR significantly improved the overall quality of renal CT images and lesion display compared with ASiR-V, even at a low dose. Therefore, DLIR is a potential denoising and reconstruction method with promising clinical value.

Acknowledgments

Funding: None.

Footnote

Conflicts of Interest: All authors have completed the ICMJE uniform disclosure form (available at https://qims.amegroups.com/article/view/10.21037/qims-22-852/coif). The authors have no conflicts of interest to declare.

Ethical Statement: The authors are accountable for all aspects of the work in ensuring that questions related to the accuracy or integrity of any part of the work are appropriately investigated and resolved. The study was conducted in accordance with the Declaration of Helsinki (as revised in 2013). The study was approved by Shandong University, and informed consent was obtained from all the patients.

References

1. Krishna S, Murray CA, McInnes MD, Chatelain R, Siddaiah M, Al-Dandan O, Narayanasamy S, Schieda N. CT imaging of solid renal masses: pitfalls and solutions. Clin Radiol 2017;72:708-21.

2. Birnbaum BA, Hindman N, Lee J, Babb JS. Multi-detector row CT attenuation measurements: assessment of intra- and interscanner variability with an anthropomorphic body CT phantom. Radiology 2007;242:109-19.
3. Chen LH, Jin C, Li JY, Wang GL, Jia YJ, Duan HF, Pan N, Guo J. Image quality comparison of two adaptive statistical iterative reconstruction (ASiR, ASiR-V) algorithms and filtered back projection in routine liver CT. Br J Radiol 2018;91:20170655.
4. Hardie AD, Nelson RM, Egbert R, Rieter WJ, Tipnis SV. What is the preferred strength setting of the sinogram-affirmed iterative reconstruction algorithm in abdominal CT imaging? Radiol Phys Technol 2015;8:60-3.
5. Geyer LL, Schoepf UJ, Meinel FG, Nance JW Jr, Bastarrika G, Leipsic JA, Paul NS, Rengo M, Laghi A, De Cecco CN. State of the Art: Iterative CT Reconstruction Techniques. Radiology 2015;276:339-57.
6. Xiao H, Teng X, Liu C, Li T, Ren G, Yang R, Shen D, Cai J. A review of deep learning-based three-dimensional medical image registration methods. Quant Imaging Med Surg 2021;11:4895-916.
7. McCollough CH, Leng S. Use of artificial intelligence in computed tomography dose optimisation. Ann ICRP 2020;49:113-25.
8. Bernard A, Comby PO, Lemogne B, Haioun K, Ricolfi F, Chevallier O, Loffroy R. Deep learning reconstruction versus iterative reconstruction for cardiac CT angiography in a stroke imaging protocol: reduced radiation dose and improved image quality. Quant Imaging Med Surg 2021;11:392-401.
9. Chartrand G, Cheng PM, Vorontsov E, Drozdzal M, Turcotte S, Pal CJ, Kadoury S, Tang A. Deep Learning: A Primer for Radiologists. Radiographics 2017;37:2113-31.
10. Alagic Z, Diaz Cardenas J, Halldorsson K, Grozman V, Wallgren S, Suzuki C, Helmenkamp J, Koskinen SK. Deep learning versus iterative image reconstruction algorithm for head CT in trauma. Emerg Radiol 2022;29:339-52.
11. Sun J, Li H, Wang B, Li J, Li M, Zhou Z, Peng Y. Application of a deep learning image reconstruction (DLIR) algorithm in head CT imaging for children to improve image quality and lesion detection. BMC Med Imaging 2021;21:108.
12. Zhou BF; Cooperative Meta-Analysis Group of the Working Group on Obesity in China. Predictive values of body mass index and waist circumference for risk factors of certain related diseases in Chinese adults--study on optimal cut-off points of body mass index and waist circumference in Chinese adults. Biomed Environ Sci 2002;15:83-96.
13. The 2007 Recommendations of the International Commission on Radiological Protection. ICRP publication 103. Ann ICRP 2007;37:1-332.
14. Thitaikumar A, Krouskop TA, Ophir J. Signal-to-noise ratio, contrast-to-noise ratio and their trade-offs with resolution in axial-shear strain elastography. Phys Med Biol 2007;52:13-28.
15. Ye K, Zhu Q, Li M, Lu Y, Yuan H. A feasibility study of pulmonary nodule detection by ultralow-dose CT with adaptive statistical iterative reconstruction-V technique. Eur J Radiol 2019;119:108652.
16. Shuman WP, Green DE, Busey JM, Kolokythas O, Mitsumori LM, Koprowicz KM, Thibault JB, Hsieh J, Alessio AM, Choi E, Kinahan PE. Model-based iterative reconstruction versus adaptive statistical iterative reconstruction and filtered back projection in liver 64-MDCT: focal lesion detection, lesion conspicuity, and image noise. AJR Am J Roentgenol 2013;200:1071-6.
17. Jensen CT, Liu X, Tamm EP, Chandler AG, Sun J, Morani AC, Javadi S, Wagner-Bartak NA. Image Quality Assessment of Abdominal CT by Use of New Deep Learning Image Reconstruction: Initial Experience. AJR Am J Roentgenol 2020;215:50-7.
18. Bailey DB. Effects of lines of progress and semilogarithmic charts on ratings of charted data. J Appl Behav Anal 1984;17:359-65.
19. Manolov R. Linear Trend in Single-Case Visual and Quantitative Analyses. Behav Modif 2018;42:684-706.
20. Jensen CT, Telesmanich ME, Wagner-Bartak NA, Liu X, Rong J, Szklaruk J, Qayyum A, Wei W, Chandler AG, Tamm EP. Evaluation of Abdominal Computed Tomography Image Quality Using a New Version of Vendor-Specific Model-Based Iterative Reconstruction. J Comput Assist Tomogr 2017;41:67-74.
21. Telesmanich ME, Jensen CT, Enriquez JL, Wagner-Bartak NA, Liu X, Le O, Wei W, Chandler AG, Tamm EP. Third version of vendor-specific model-based iterativereconstruction (Veo 3.0): evaluation of CT image quality in the abdomen using new noise reduction presets and varied slice optimization. Br J Radiol 2017;90:20170188.

Cite this article as: Bie Y, Yang S, Li X, Zhao K, Zhang C, Zhong H. Impact of deep learning-based image reconstruction on image quality and lesion visibility in renal computed tomography at different doses. Quant Imaging Med Surg 2023;13(4):2197-2207. doi: 10.21037/qims-22-852

